Sensors and Materials, Vol. 35, No. 7 (2023) 2399–2411
MYU Tokyo

S & M 3331

Microwave Imaging of Conductors by Direct Sampling Method and U-Net

Chien-Ching Chiu,[1*] Ching-Lieh Li,[1] Wei Chien,[2] Hong-Yu Wu,[1]
Po Hsiang Chen,[1] Eng Hock Lim,[3] and Guo-Zheng Chen[1]

[1]Department of Electrical and Computer and Engineering, Tamkang University, New Taipei City 251301, Taiwan
[2]Department of Computer Information and Network Engineering, Lunghwa University of Science and Technology, Taoyuan City 333326, Taiwan
[3]Department of Electrical and Electronic Engineering, University Tunku Abdul Rahman, Kajang 43200, Malaysia

(Received April 7, 2023; accepted June 26, 2023)

Keywords: inverse scattering, frequency domain, conductor, direct sampling method, U-Net

Electromagnetic imaging is an emerging technology widely applied in many fields, such as medical imaging, biomedical imaging, and nondestructive testing. In this study, we place transmitter and receiver antennas around an unknown object. We can use the direct sampling method (DSM) to reconstruct the material size and shape of the unknown object on the basis of the scattered field. We apply U-Net to reconstruct electromagnetic images of perfect conductors. Perfect conductors in free space are studied by irradiating a transverse magnetic (TM) polarization wave. Using the scattered electric field measured outside the object together with the boundary conditions on the conductor surface, a set of nonlinear integral equations can be derived and further converted into matrix form by the method of moments. Since an iterative algorithm is computationally expensive and time-consuming, a real-time electromagnetic imaging technique combining deep learning neural networks is proposed for reconstructing the perfect conductors. The initial shapes of the conductors are first computed by DSM by using the scattered electric field measured outside the object. The initial shapes of the conductors are then input to U-Net for training. Numerical results show that U-Net is capable of reconstructing accurate conductor shapes. Therefore, artificial intelligence techniques can reconstruct shapes more accurately than iterative algorithms, when combined with DSM.

1. Introduction

In recent years, electromagnetic imaging has been used in a large number of underground gas pipes and in electrical high-voltage cable detection and medical imaging by methods such as computed tomography and magnetic resonance imaging. Particularly in medical imaging, the technology is superior to X-ray imaging, and the ability to collect scattered field information is much greater than that when using X-ray equipment. This has drawn the attention of scholars, leading to significant progress in recent years. The microwave imaging technique still has urgent research issues such as poor penetration results when the signal-to-noise ratio is low, ill-posedness, nonlinearity, and large computational burden, as well as the parameter selection

*Corresponding author: e-mail: chiu@ee.tku.edu.tw
https://doi.org/10.18494/SAM4446

ISSN 0914-4935
https://myukk.org/

problem. To conquer the above problems, the inverse scattering problem is generally converted to an optimization problem, which can be solved by the 1) objective function method[1–17] or 2) neural network learning method.[8–22] The objective function is generally used to find the extreme value of the problem, e.g., to calculate the minimum error of the scattering field and the measured scattering field. The gradient method is more suitable for small-area searches,[4] whereas the global algorithm is suitable for full-area searches.[2] The whale optimization algorithm was applied to the inverse scattering of an imperfect conductor with corners in 2020.[6] The effect of incident field polarization was analyzed for inverse metal object scattering by discrete dipole approximation.[7] The simulation results indicate that a circularly polarized wave is superior for obtaining better imaging results.

Regarding the neural network learning method,[8–22] Yao *et al.* used a two-stage neural network, in which the preliminary permittivity from the scattering field in the first stage and then the neural network was used to calculate the true permittivity.[10] Wei and Chen proposed a deep learning method to improve the results. The proposed method improved the accuracy of the reconstructed images by calculating the dominant currents scheme to estimate the dielectric constant, and then reconstructed the true dielectric constant using the convolutional neural network.[11] Yin *et al*. devised a quantitative inversion scheme of alternately updating the contrast of dielectric scatterers and the T-matrix of conductors for electromagnetic imaging.[19] Liu *et al*. proposed new designs of loss functions that incorporate multiple scattering using near-field quantities to reconstruct the permittivity.[21] Effects of physics-guided loss functions were studied through various numerical experiments. A deep learning convolutional neural network architecture for the shape imaging of perfectly electrically conducting rough surfaces was addressed in Ref. 22. The algorithm was numerically tested with various scenarios and proved to be very effective.

To the best of our knowledge, there is no numerical result for perfect conductors obtained using U-Net. The inverse scattering problem was normally solved by an iterative algorithm in the past. However, the drawback of this algorithm is that it is highly time-consuming and computationally costly. In addition, the result reconstructed by inputting the scattered field directly into U-Net is not satisfactory because U-Net is only effective for image processing. The innovation of our study is that the initial image is first estimated by DSM before being reconstructed by U-Net. Numerical results show that our proposed method is efficient as well as highly accurate. In this work, the inverse problem of perfect conductors is tackled using U-Net with initial shape estimation by DSM. In Sect. 2, solutions to the direct and inverse problems are presented. In Sect. 3, the convolutional neural network with the U-Net framework used in this study is described. Numerical results of solving the proposed inverse problem are given in Sect. 4. In Sect. 5, we present our conclusions.

2. Direct and Inverse Problems

Consider a perfect conductor located in free space. Assume that the conductor extends infinitely in the z-axis direction and that its cross-sectional area in the (x, y) plane can be expressed by the polar coordinates equation $\rho = F(\theta)$, as shown in Fig. 1.

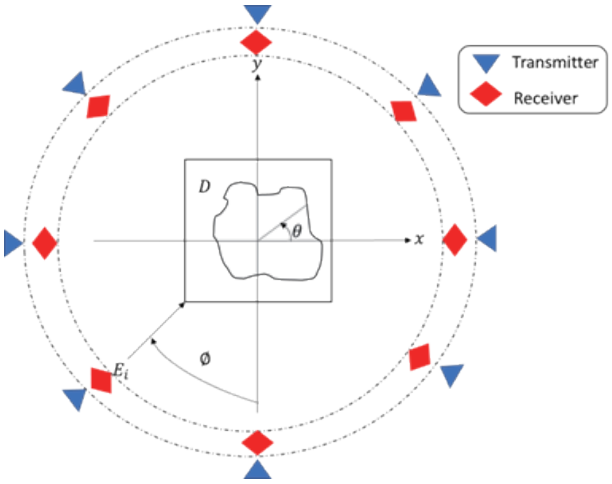

Fig. 1. (Color online) Geometry of electromagnetic problem in a plane.

The permittivity in free space is denoted as ϵ_0 and the permeability is denoted as μ_0. The harmonic wave of the form $e^{j\omega t}$ is assumed and the incident electric field is assumed to be parallel to the z-axis, i.e., waves are TM-polarized. The incident field with the incident angle $\varnothing$ is represented by $\overline{E_i}$, as expressed by

$$\overline{E_i}(x,y) = e^{-jk\left(x\sin\varnothing\sqrt{2}+y\cos\varnothing\right)}\hat{z},\ k^2 = \omega^2\varepsilon_0\mu_0, \tag{1}$$

where k is the wave number in free space. The electromagnetic field satisfies Maxwell's equation and the only component of the electric field is in the z-direction. We can treat the scattered electric field $\overline{E_s} = E_s\hat{z}$ as the radiation of the induced surface current J_S. By considering the two-dimensional Green's function, the scattered field at any point (x, y) outside the conductor can be expressed as

$$\begin{aligned} E_S(x,y) &= -\int_0^{2\pi} G_0(x,y;x',y')\cdot J(\theta')d\theta' \\ &= -\int_0^{2\pi} \frac{j}{4}H_0^{(2)}\left[k\sqrt{\left(x-F(\theta')\cos\theta'\right)^2+\left(y-F(\theta')\sin\theta'\right)^2}\right]\cdot J(\theta')d\theta', \end{aligned} \tag{2}$$

$$G_0(x,y;x',y') = \frac{j}{4}H_0^{(2)}\left[k\sqrt{(x-x')^2+(y-y')^2}\right], \tag{3}$$

$$J(\theta) = -j\omega\mu_0\sqrt{F^2(\theta)+F'^2(\theta)}J_S(\theta), \tag{4}$$

where G_0 is Green's function in free space and $H_0^{(2)}$ is the zero-order Hankel function of the second type. $J(\theta)$ is proportional to the surface current. In Eq. (2), when the measurement distance is large enough, the scattering field can be expressed in asymptotic form.

$$E_s(x,y) \approx \frac{e^{-jkr}}{\sqrt{r}} I_s(\theta) \tag{5}$$

$$I_s(\theta) = -\frac{j}{4}\sqrt{\frac{2}{\pi k}} e^{\frac{j\pi}{4}} \int_0^{2\pi} e^{jkF(\theta')\cos(\theta-\theta')} J(\theta') d\theta' \tag{6}$$

$I_s(\theta)$ is the well-known scattering far-field pattern.

The boundary condition of perfect conductors is that the tangential component of the total electric field on the surface of the conductor is zero.

$$\hat{n} \times \vec{E} = 0 \tag{7}$$

Here, $\hat{n}$ is the unit vector perpendicular to the conductor, pointing outward from the conductor. On the basis of this boundary condition, we can derive the integral equation of $J(\theta)$.

$$E_i\left(F(\theta),\theta\right) = \int_0^{2\pi} \frac{j}{4} H_0^{(2)}\left(kr_0\right) J(\theta') d\theta' \tag{8}$$

$$r_0(\theta,\theta') = \left[F^2(\theta) + F^2(\theta') - 2F(\theta)F(\theta')\cos(\theta-\theta')\right]^{\frac{1}{2}} \tag{9}$$

For the direct scattering problem, the shape of the target is known, and we want to find the value of the scattering field. We first solve $J(\theta)$ in Eq. (8) and then substitute $J(\theta)$ into Eq. (2) to obtain the scattering field E_S. To complete the calculation of direct scattering numerically, we use the method of moments to solve Eqs. (2) and (8). In the first step, the pulse function is used to develop $J(\theta)$.

$$J(\theta) \cong \sum_{n=1}^{M_d} B_n P_n(\theta) \tag{10}$$

$$P_n(\theta) = 1, \text{ on } \Delta C_n \tag{11}$$

$$P_n(\theta) = 0, \text{ on all other } \Delta C_m \tag{12}$$

ΔC_i represents the ith arc segment of the object from $\theta = 2\pi(i-1)/M_d$ to $\theta = 2\pi/M_d$. The number of segments, M_d, used to expand $J(\theta)$ must be large enough that $J(\theta)$ can be considered constant in the region of each segment ΔC_i. Since $J(\theta)$ is a finite pulse function, the role of regularization is implied.

The Dirac delta function is also selected as the test function.

$$V_m \triangleq \delta\left(\theta - \theta_m\right) \tag{13}$$

$$\theta_m = \frac{2\pi m}{M} \quad m = 1, 2, \cdots, M_d \tag{14}$$

Then, Eq. (8) can be reduced to

$$\left\langle E_i\left(F\left(\theta\right),\theta\right), V_m \right\rangle = \left\langle \int_0^{2\pi} \frac{j}{4} H_0^{(2)}\left(kr_0\right) J\left(\theta'\right) d\theta', V_m \right\rangle \tag{15}$$

or

$$\left\langle E_i\left(F\left(\theta\right),\theta\right), V_m \right\rangle = \left\langle \int_0^{2\pi} \frac{j}{4} H_0^{(2)}\left(kr_0\right) J\left(\theta'\right) d\theta', V_m \right\rangle. \tag{16}$$

Similarly, Eq. (2) can be reduced to

$$E_s\left(\vec{r}\right) = -\sum_{n=1}^{M_d} B_n \int_{\Delta C_n} \frac{j}{4} H_0^{(2)}\left[k\sqrt{\left(x - F\left(\theta'\right)\cos\theta'\right)^2 + \left(y - F\left(\theta'\right)\sin\theta'\right)^2}\right] d\theta'. \tag{17}$$

DSM is a noniterative sampling-type technique for retrieving the shape and position of an unknown scatterer.[14] It was first applied to two-dimensional dielectric inverse scattering problems with fixed-plane incident waves and later extended to various inverse scattering problems. DSM is a fast method because it does not require additional operations such as singular value decomposition or the solving of ill-posed integral equations. More importantly, it is robust to random noise. The DSM formula for the indicator function is given as

$$\Psi\left(r_p\right) = \frac{1}{N_i} \sum_{l=1}^{N_i} \frac{\left|\overline{E_s^l}\left(r\right), \overline{G_0}\left(r, r_p\right)\right|}{\overline{E_s^l}\left(r\right) \overline{G_0}\left(r, r_p\right)}, \tag{18}$$

where r_p is a single sampling point, r is the receiver position with a total of N_r receiver points, and N_i is the number of transmitters. $\overline{E_s^l}\left(r\right)$ is the vector of $N_r \times 1$ and $\overline{G_0}\left(r, r_p\right)$ is the vector of $N_r \times 1$. If $\Psi(r_p) \approx 1$, the sampling point r_p is within the unknown scatter and, if $\Psi(r_p) \approx 0$, the sampling point r_p belongs to the background medium.[14]

3. Convolutional Neural Networks (CNNs)

A CNN is a neural network that has one or more convolution layers. Convolution means to slide a filter over the input, rather than looking at the full image at once, in order to extract the features of the input image. It can be more effective to look at smaller portions of the image. The CNN is made up of four types of layers: a convolution layer, a pooling layer, a rectified linear unit (ReLU) layer, and a fully connected layer. The mathematical operation of the convolution layer is carried out by different convolution kernels on the input image. The pooling layer is responsible for the reduction of the image of the convolved feature, thus reducing the number of training parameters and avoiding overfitting. The fully connected layer, where each node is connected to all precious nodes, predicts the image's class based on the features. The ReLU layer enhances the functional judgment and nonlinear properties of the neural network. The image segmentation method of the CNN proposed by the University of Freiburg, Germany, is used in this study.[8] Figure 2 shows the U-Net architecture. It comprises the left half of the shrinkage network and the right half of the expansion network, including repeated additions of a 3 × 3 convolution layer, a batch normalization layer, and a ReLU layer. In addition, a 2 × 2 max-pooling layer in the shrinkage network and a 3 × 3 transposed convolution layer in the expansion network are used. However, the largest difference between the shrinkage and expansion network architectures for the transposed convolution layer is that the 1 × 1 convolution layer is used in the fully connected layer. After averaging the outputs of the fully connected layer, the average is input to the regression layer to calculate the error of the shape. The minimum equation is expressed as

$$\underset{A_i,i}{\operatorname{argmin}} : \sum_{N=1}^{N_t} H\left(A_i\left(F(\theta)^{\alpha}\right), F(\theta)\right) + Q(i), \tag{19}$$

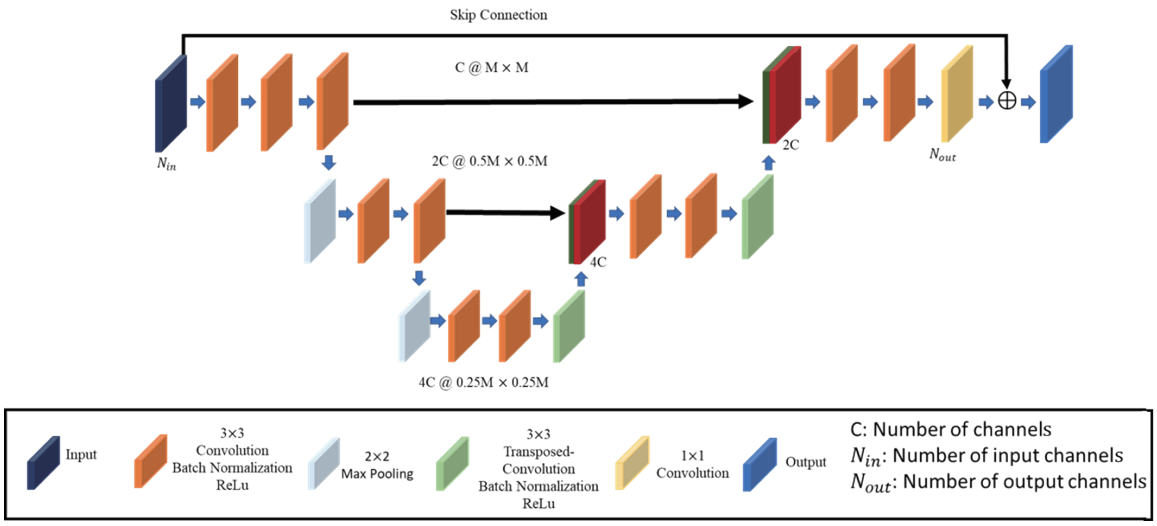

Fig. 2. (Color online) U-Net architecture.

where A_i represents the neural network structure, i represents the parameter of the neural network, H represents the error, $F(\theta)^{\alpha}$ and $F(\theta)$ represent the approximate and exact shapes respectively, and $Q(i)$ represents the regular function. N_t is the number of equivalent effective incidences.

4. Numerical Results

Numerical analysis for the imaging problem of perfect conductors in free space has been presented. The TM-polarized incident wave with a frequency of 3GHz is employed to illuminate the conductors. 5% Gaussian noise is added to the environment. The receivers and transmitters at 18-degree intervals are placed uniformly along a circle with a radius of 3m. As a result, a total of 20 receivers and 20 transmitters are used in the environment.

The domain of interest is 0.16 m × 0.16 m which is divided into a 64 × 64 pixel area. Conductors with different shapes are placed randomly in the domain. There is a total of 3024 dataset images. In other words, the 3024 initial-guess images are generated by DSM and the corresponding original images are input to U-Net as the datasets. The dataset images are split into 80% training images and 20% testing images. The number of channels, C, is set to 64.

The learning rate is set from 10^{-6} to 10^{-8} for a stochastic gradient descent momentum. The maximum epoch is set as 200 while the data are reshuffled in every epoch of training. The root mean square error (RMSE) is used to show the discrepancy and is defined as

$$RMSE = \frac{1}{M_t}\sum_{i=1}^{M_t}\left\|S - S^{\alpha}\right\|_{FO} / \left\|S\right\|_{FO}, \tag{20}$$

where S and S^{α} are the original and reconstructed shapes, respectively, M_t is the test number, and FO denotes the Frobenius norm.

To compare the reconstruction results of all graphs, the structural similarity index measure (SSIM) for evaluating the graph trained by U-Net is defined as

$$SSIM = \frac{\left(2\mu_{\tilde{y}}\mu_y + C_1\right)\left(2\sigma_{\tilde{y}y} + C_2\right)}{\left(\mu_{\tilde{y}}^2 + \mu_y^2 + C_1\right)\left(\sigma_{\tilde{y}}^2 + \sigma_y^2 + C_2\right)}, \tag{21}$$

where $\tilde{y}$ and y are the reconstructed and original shapes, respectively. μ_y is the pixel sample mean of y, σ_y^2 is the variance of y, and $\sigma_{\tilde{y}y}$ is the covariance of $\tilde{y}$ and y. C_1 and C_2 are two variables for stabilizing the division with a weak denominator.

Figure 3(a) shows the original apple shape and Fig. 3(b) the image reconstructed by U-Net. We can see that the reconstruction is slightly imperfect at the edge of the shape. The RMSE is about 4.9% and the SSIM is about 95.8%, as shown in Table 1.

Figure 4(a) shows the original butterfly shape and Fig. 4(b) the image reconstructed by U-Net. It is seen that there is a minor difference at the right bottom part of the shape. The RMSE is about 6.0% and the SSIM is about 94.8%, as shown in Table 1.

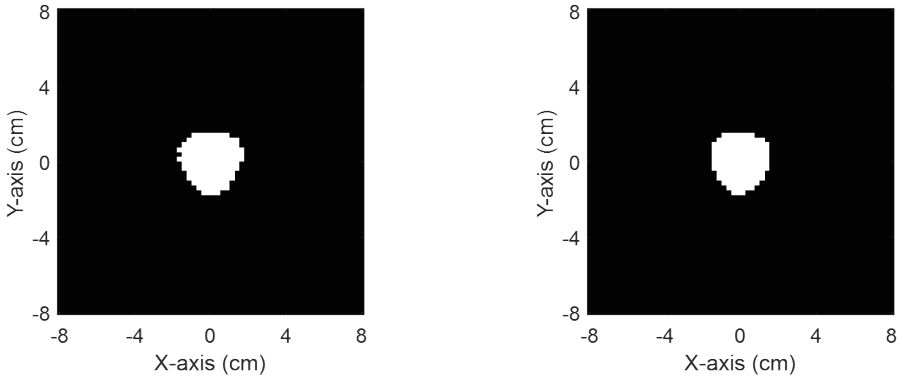

Fig. 3. Reconstruction example 1. (a) Original shape. (b) Reconstructed shape.

Table 1
RMSE and SSIM values of various shapes.

Performance	Case					
	Apple	Butterfly	Circle	Peanut	Petal	Mushroom
RMSE (%)	4.9	6.0	6.5	6.8	7.5	7.5
SSIM (%)	95.8	94.8	94.3	93.6	93.4	92.7

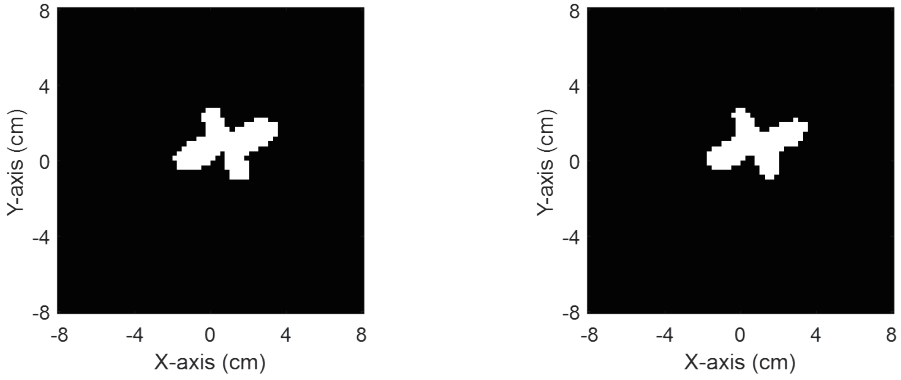

Fig. 4. Reconstruction example 2. (a) Original shape. (b) Reconstructed shape.

Figure 5(a) shows the original circle shape and Fig. 5(b) the image reconstructed by U-Net. It is seen that there is a slight error at the top left part of the shape. The RMSE is about 6.5% and the SSIM is about 94.3%, as shown in Table 1.

Figure 6(a) shows the original peanut shape and Fig. 6(b) the image reconstructed by U-Net. The two are almost the same except that the right side of the reconstructed shape is smaller than that of the original shape. The RMSE is about 6.8% and the SSIM is about 93.6%, as shown in Table 1.

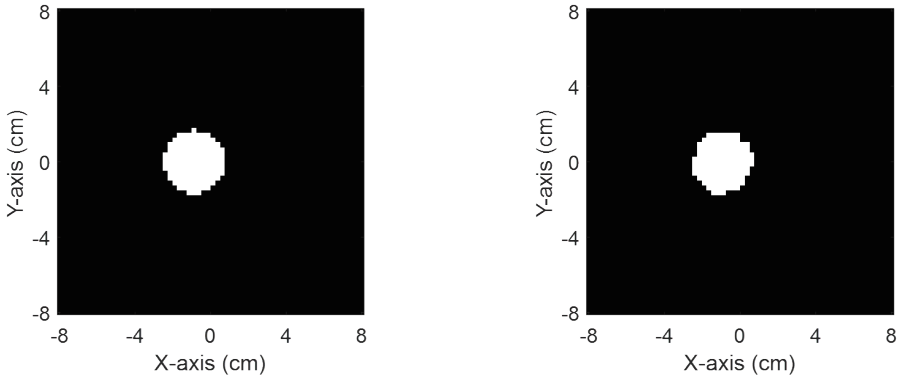

Fig. 5. Reconstruction example 3. (a) Original shape. (b) Reconstructed shape.

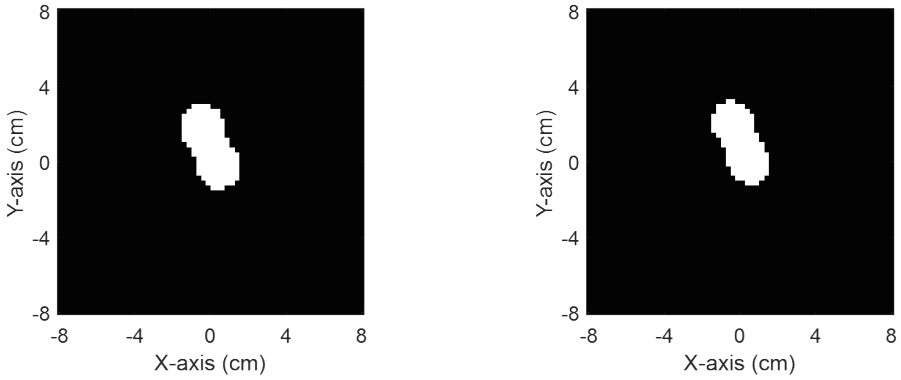

Fig. 6. Reconstruction example 4. (a) Original shape. (b) Reconstructed shape.

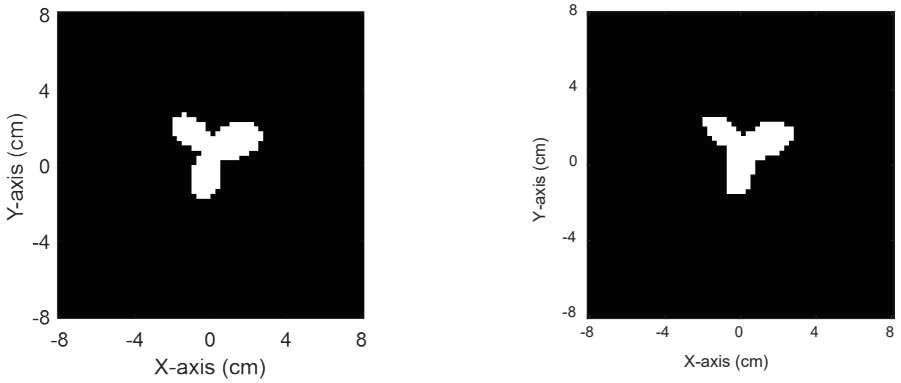

Fig. 7. Reconstruction example 5. (a) Original shape. (b) Reconstructed shape.

Figure 7(a) shows the original three-petal shape and Fig. 7(b) the image reconstructed by U-Net. As shown, there are some inaccuracies at the bottom right of the shape. The RMSE is about 7.5% and the SSIM is about 93.4%, as shown in Table 1.

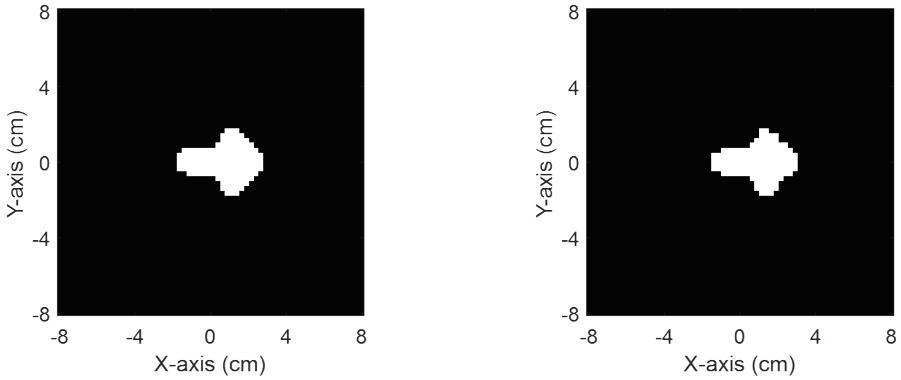

Fig. 8. Reconstruction example 6. (a) Original shape. (b) Reconstructed shape.

Figure 8(a) shows the original mushroom shape and Fig. 8(b) the image reconstructed by U-Net. We observe some errors on the left, right and upper parts of the shape. The RMSE is about 7.5% and the SSIM is about 92.7%, as shown in Table 1.

5. Conclusion

In this paper, we presented the reconstruction performance for perfect conductors by U-Net. First, we adopted the concept of induced currents to derive the integral equation for the scattering field and solved it by the method of moments. Next, we applied DSM to find the preliminary shapes of perfect conductors. Then, we applied U-Net to obtain a more accurate reconstruction. From the results of our numerical simulation, we found that, in spite of the high noise level, better reconstruction for perfect conductors was achieved when artificial intelligence technology was employed for the inverse scattering problem. Our proposed method can be used for nondestructive testing, mine detection, magnetic resonance imaging, and medical imaging.

References

1 S. D. Meo, P. F. Espín-López, A. Martellosio, M. Pasian, G. Matrone, M. Bozzi, G. Magenes, A. Mazzanti, L. Perregrini, F. Svelto, P. E. Summers, G. Renne, L. Preda, and M. Bellomi : IEEE Trans. Micro. Theory Tech. **65** (2017) 1795. https://doi.org/10.1109/TMTT.2017.2672938
2 C. C. Chiu, G. Z. Lee, H. Jiang, and B. J. Hong: J. Electron. Waves Appl. **33** (2019) 1905. https://doi.org/10.1080/09205071.2019.1653229
3 Z. Miao and P. Kosmas: IEEE Trans. Antennas Propaga. **65** (2017) 2507. https://doi.org/10.1109/TAP.2017.2679067
4 Y. Zhong, M. Salucci, K. Xu, A. Polo, and A. Massa: IEEE Trans. Micro. Theory Tech. **68** (2020) 1234. https://doi.org/10.1109/TMTT.2019.2956939
5 B. L. P. Meenaketan, S. Pal, and N. Chattoraj: Int. J. RF Micro. Comput. Aided Eng. **29** (2019) 21908. https://doi.org/10.1002/mmce.21908
6 K. C. Lee and P. T. Lu: Int. J. Antennas Propaga. **2020** (2020) 1. https://doi.org/10.1155/2020/8205797
7 X. Zheng and B. Hu: Proc. 13th Int. Symp. Antennas Propaga. EM Theory (ISAPE 2021) 1–3.
8 O. Ronneberger, P. Fischer, and T. Brox: Proc. Med. Image Comput. Comput.-Assist. Inter. (MICCAI 2015) 234–241.

9 X. Chen, Z. Wei, M. Li, and P. Rocca: Prog. Electron. Res. **167** (2020) 67. https://doi.org/10.2528/PIER20030705
10 H. M. Yao, W. E. I. Sha, and L. Jiang: IEEE Antennas Wireless Propaga. Lett. **18** (2019) 2254. https://doi.org/10.1109/LAWP.2019.2925578
11 Z. Wei and X. Chen: IEEE Trans. Geo. Remote Sens. **57** (2019) 1849. https://doi.org/10.1109/TGRS.2018.2869221
12 Z. Wei and X. Chen: IEEE Trans. Antennas Propaga. **67** (2019) 6138. https://doi.org/10.1109/TAP.2019.2922779
13 W. Shao and Y. Du: IEEE Trans. Antennas Propaga. **68** (2020) 5626. https://doi.org/10.1109/TAP.2020.2978952
14 L. Zhang, K. Xu, R. Song, X. Ye, G. Wang, and X. Chen: IEEE Sens. J. **20** (2020) 15007. https://doi.org/10.1109/JSEN.2020.3012177
15 P. Mojabi, M. Hughson, V. Khoshdel, I. Jeffrey, and J. LoVetri: IEEE J. Multis. Multip. Comp. Tech. **6** (2021) 62. https://doi.org/10.1109/JMMCT.2021.3076827
16 Z. Ma, K. Xu, R. Song, C. F. Wang, and X. Chen: IEEE Trans. Antennas Propaga. **69** (2021) 2194. https://doi.org/10.1109/TAP.2020.3026447
17 K. Xu, C. Zhang, X. Ye, and R. Song: IEEE Trans. Geo. Remote Sens. **60** (2022) 1. https://doi.org/10.1109/TGRS.2021.3093100
18 X. Ye, D. Yang, X. Yuan, R. Song, S. Sun, and D. Fang: IEEE Trans. Antennas Propaga. **70** (2022) 8262. https://doi.org/10.1109/TAP.2022.3164198
19 F. Yin, C. Chen, and W. Chen: IEEE Trans. Antennas Propaga. **70** (2022) 3643. https://doi.org/10.1109/TAP.2021.3137294
20 T. Hanabusa, T. Morooka, and S. Kidera: IEEE Geo. Remote Sens. Lett. **19** (2022) 1. https://doi.org/10.1109/LGRS.2022.3169799
21 Z. Liu, M. Roy, D. K. Prasad, and K. Agarwal: IEEE Trans. Comput. Imag. **8** (2022) 236. https://doi.org/10.1109/TCI.2022.3158865
22 İ. Aydin, G. Budak, A. Sefer, and A. Yapar: Int. J. Remote Sens. **15**–**16** (2022) 5527. https://doi.org/10.1080/01431161.2022.2105177

About the Authors

Chien-Ching Chiu received his B.S.C.E. degree from National Chiao Tung University, Hsinchu, Taiwan, in 1985 and his M.S.E.E. and Ph.D. degrees from National Taiwan University, Taipei, in 1987 and 1991, respectively. From 1987 to 1989, he was a communication officer with the ROC Army Force. In 1992, he joined the Department of Electrical Engineering, Tamkang University, where he is now a professor. From 1998 to 1999, he was a visiting scholar at Massachusetts Institute of Technology, Cambridge, and the University of Illinois at Urbana-Champaign, USA. He was a visiting professor at the University of Wollongong, Australia, in 2006, the University of London, United Kingdom, in 2011, and University Tunku Abdul Rahman, Malaysia, from 2019 to 2020. His current research interests include inverse problems, deep learning for microwave imaging, indoor wireless communications, and simultaneous wireless information and power transfer systems. He has published more than 150 journal papers on inverse scattering problems, communication systems, and optimization algorithms. (chiu@ee.tku.edu.tw)

Ching-Lei Li received his B.S. degree from National Taiwan University, Taipei, Taiwan, in 1985, and M.S. and Ph.D. degrees from Michigan State University, East Lansing, in 1990 and 1993, respectively, all in electrical engineering. From 1989 to 1993, he was a research assistant in the Electrical Engineering Department, Michigan State University, where he worked on measurement techniques for determining the electromagnetic properties of materials. In 1993, he joined the Electrical Engineering Faculty at Tamkang University, Taipei, where he is now a professor. Currently, his research activities involve the inverse scattering problem, microstrip antenna design, and dielectric material characterization. His areas of special interest include theoretical and computational electromagnetics, the application of various optimization schemes, such as the steady-state genetic algorithm, particle swarm optimization, differential evolution, and Taguchi method, to electromagnetics, recent emerging research areas including applications of artificial intelligence in electromagnetics, and other topics.
(chingliehli1001@gms.tku.edu.tw)

Wei Chien received his B.S.C.E. degree from Ta Tung University, Taipei, in 1997 and his M.S.E.E. degree from Tamkang University, Taipei, in 1999. From 1999 to 2001, he served in the ROC Army Force and was an assistant in the Department of Electrical Engineering. From 2007 to 2014, he was an assistant professor in the Department of Electronic Engineering, De Lin Institute of Technology. From 2014 to 2017, he was a professor in the Department of Computer Engineering, Ningde Normal University. Since 2017, he has been a professor in the Department of School of Electric and Information Engineering, Beibu Gulf University. His research area is deep learning for inverse scattering. (air180@seed.net.tw)

Hung-Yu Wu majored in computer science and electrical engineering. He received his master's degree in electrical engineering in 1999. He is a firewall programmer for products such as laser printers, digital set-top-boxes, and credit card machines. Currently, he is exploring indoor wireless communication systems that include MIMO, beamforming, and wireless power transfer technologies, as well as optimization algorithms, such as GA, SADDE, APSO, and neural networks. (807440036@gms.tku.edu.tw)

Po-Hsiang Chen received his B.S. degree from HungKuo Delin University of Technology, Tucheng, Taiwan, in 2017 and M.S. degree from Tamkang University, Tamsui, Taiwan, in 2020. Since 2021, he has been working toward his Ph.D. at the Department of Electrical and Computer Engineering, Tamkang University, Tamsui, Taiwan. His research areas are inverse scattering and deep learning. (810440031@gms.tku.edu.tw)

Eng Hock Lim (Senior Member, IEEE) received his B.Sc. degree in electrical engineering from National Taiwan Ocean University in 1997, M.Eng. degree in electrical and electronic engineering from Nanyang Technological University in 2000, and Ph.D. degree in electronic engineering from the City University of Hong Kong in 2007. He is currently a professor with Universiti Tunku Abdul Rahman (UTAR), Malaysia. His current research interests include RFID antennas, reflect arrays, transmit arrays, and multifunctional antennas. He is also the Founding Chair of the IEEE Council on RFID, Malaysia Chapter. He served as an associate editor for IEEE Transactions on Antennas and Propagation from 2013 to 2016. (limeh@utar.edu.my)

Guo-Zhang Chen received his B.S. degree from HungKuo Delin University of Technology, Tucheng, Taiwan, in 2020 and M.S. degree from Tamkang University, Tamsui, Taiwan, in 2022. He is dedicated to inverse scattering and deep learning research. (609440051@gms.tku.edu.tw)